Integrating SMART principles in Flood Early Warning System Design in the Himalayas

Author: Sudhanshu Dixit[1], Sumit Sen[1*], Tahmina Yasmin[2], Kieran Khamis[2], Debashish Sen[3], Wouter Buytaert[4], David M. Hannah[2]

[1]Centre of Excellence in Disaster Mitigation and Management, Indian Institute of Technology Roorkee, Roorkee, Uttarakhand, India
[2]School of Geography, Earth & Environmental Sciences, University of Birmingham, Birmingham, UK
[3]People's Science Institute, Dehradun, India
[4]Department of Civil and Environmental Engineering, Imperial College London, London, UK
*Correspondence to sumit.sen@hy.iitr.ac.in

Abstract

Extreme precipitation events have increased community and asset vulnerability to hazards like flash floods, particularly in mountainous regions. In response, this study adopts SMART principles emphasizing inclusiveness and a bottom-up, community-led approach towards the development of an urban flood early warning system (EWS) in the Lesser Himalayas. The study demonstrates how low-cost, community-engaged hydrometeorological monitoring can capture the nuances of catchment and storm characteristics to improve urban flood early warning in data-scarce mountain regions. A hydrometeorological monitoring network comprising three LiDAR-based water-level sensors and four rain gauges was deployed across the Bindal watershed, Uttarakhand, India. Observations reveal pronounced spatial variability, as seen in September 2022, with rainfall differences of 187 mm and inter-station correlations ranging from r = 0.82 to 0.20 over distances of 2.74-8.24 km. A southwestward movement of rainfall systems with an approximate 15-minute lag was also observed within the watershed. In contrast, secondary datasets (GPM-IMERG and ERA5) failed to capture the magnitude and heterogeneity of precipitation patterns, raising concerns about their reliability for flash flood studies in mountainous areas. These findings underscore the advantage of SMART approach integrating hydrometeorological insights, utilizing low-cost monitoring systems, and community engagement to strengthen urban flood resilience in Himalayan regions.

Keywords: Flood Early Warning System, Flash flood, Himalayas, Rainfall variability

1. Introduction

Climate change and water are intrinsically linked, as global warming disrupts the hydrological cycle's balance. It alters rainfall patterns, increases the frequency of extreme rainfall events, and amplifies variability and unpredictability. (Kulkarni & Agarwal, 2024; Liu et al., 2020; Shi et al., 2021; Upadhyay et al., 2023). Global analysis of daily rainfall records from 1964 to 2013 shows a consistent rise in the intensity and frequency of extreme precipitation events (Papalexiou & Montanari, 2019). These extreme rainfall events often trigger devastating floods and droughts, threatening both lives and infrastructure. A recent global study highlights that 1.81 billion people 23% of the world's population are directly exposed to 1-in-100-year flood events. Most of this at-risk population, around 1.24 billion, live in South and East Asia, with China (395 million) and India (390 million) together accounting for over one-third of global flood exposure (Rentschler et al., 2022). These numbers underscore the critical need for robust Disaster Risk Reduction (DRR) strategies to manage the heightened risks associated with floods.

Flash floods (FFs) are characterized by a rapid and intense surge of water over a localized area (National Weather Service, US), posing unique challenges for mitigation. The distinct short time scales and occurrence on small spatial scales differentiate FFs from other floods, exhibiting rapid onset with minimal lead time for prediction (Collier, 2007; Das et al., 2022). FFs rank among the world's deadliest natural disasters (> 5000 deaths annually), constituting approximately 85% of flooding cases and bearing the highest mortality rate among different classes of flooding (Flash Flood Guidance System, WMO). They are driven by several key factors, including intense rainfall that exceeds the ground's absorption capacity, the duration and amount of rainfall, and the spatial-temporal distribution of rainfall, all leading to rapid runoff. In addition to rainfall characteristics, local factors such as urbanization, steep terrain, soil type, and vegetation cover also play a major role (Henao Salgado & Zambrano Nájera, 2022; Hoang & Liou, 2024; Jodar-Abellan et al., 2019; Wang et al., 2023). Rapid urbanization exacerbates the impact, introducing non-stationarity in precipitation extremes through the reduced soil permeability, enhanced convection, and altered impact of large-scale climate circulations (Qian et al., 2022; Song et al., 2022) The urban heat island effect also contributes by raising temperatures in urban areas, further influencing precipitation extremes (Gu et al., 2019; Shepherd et al., 2010; Singh et al., 2013). Furthermore, there was a significant increase in the global urban population, with the proportion rising from 30% in 1950 to 55% in 2018, and it is projected to increase to 68% by 2050 (UN, 2018). Therefore, the climate change along with rapid urbanization intensify the severity and unpredictability of extreme precipitation events, resulting in complex runoff generation mechanisms and devastating FFs(Lei et al., 2024).

In the Himalayas, the severity of FFss are exacerbated by steep topography, intense rainfall, rapid snowmelt, and fragile ecosystem presenting considerable threat to life and property (Rasmussen & Houze, 2012; Satendra et al., 2015). States along the southern Indian Himalayas, such as Himachal Pradesh, Sikkim, and Uttarakhand, are experiencing growing risks from FFs, mainly driven by intense and erratic rainfall (Dimri et al., 2016). The interplay between evolving climatic conditions and rapid urbanization exacerbates these risks, emphasizing the necessity for enhanced forecasting and mitigation strategies to safeguard vulnerable populations in the Himalayan region (Arlikatti et al., 2018). Developing effective flood Early Warning Systems (EWS) is essential for addressing the vulnerability of Himalayan watersheds to FFs. EWS is a critical component of the Disaster Risk Reduction (DRR) framework, which aims to minimize the impact of natural hazards and enhance preparedness. Various approaches have been proposed to detect and predict FFs with increased accuracy and lead time (Bloschl et al., 2008; Hapuarachchi et al., 2011; N. Zhou et al., 2024), including conventional flood monitoring systems with limited range and sophistication (Zakaria & Jabbar, 2021). However, major sources of uncertainty in EWS are due to:

1. Lack of high-resolution reliable rainfall observations, as they are crucial in accurate flood predictions but are scarce in high altitude regions like the Himalayas (Chawla & Mujumdar, 2020; Gebrechorkos et al., 2024);

2. Challenges with secondary datasets - Satellite and reanalysis data face resolution and accuracy issues due to high altitude and complex steep terrain (Dogra et al., 2023);
3. Limited knowledge of hydrological processes - Insufficient knowledge of hydrological dynamics in complex Himalayan watersheds results in inaccuracy of predictive models (Nanda et al., 2018; Nepal et al., 2014)
4. Lack of inclusiveness - When the local community is not involved, it weakens local resilience and reduces the ability of the system to address diverse socio-economic vulnerabilities.

Addressing these challenges is crucial for enhancing the reliability and functionality of Flood EWS (Ward et al., 2011; Yasmin et al., 2023; Zakaria & Jabbar, 2021).

Therefore, the present work emphasizes adopting SMART approach (Shared understanding of risks, Monitoring of risks, building Awareness, Response action on Time) proposed by (Yasmin et al., 2023) , which promotes inclusiveness and a bottom-up strategy to maximize local relevance and effectiveness. Community involvement strengthens EWS

by integrating local knowledge into system design and decision-making. Unlike traditional statistical models that rely on fixed thresholds, a community-driven approach allows for the dynamic determination and regular adjustment of warning thresholds based on changing river channel conditions. This makes flood warnings better suited for the local conditions, flexible, and ultimately more reliable for decision making.

The present study, building on the principles of the SMART approach and the dynamical thresholding, takes a step towards enhancing flood EWS in urban, mountainous Himalayan regions, where data availability is limited and watershed characteristics exhibit high variability. The primary objectives of this work are: 1) to demonstrate the benefits of low-cost, real-time monitoring systems and the importance of fostering community engagement in flood risk management; and 2) to integrate the spatiotemporal variability and dynamic nature of watershed characteristics into flood EWS. The findings of our study are anticipated to develop adaptive and context-specific flood nowcasting approaches, serving as an essential step towards effective and localized flood risk management

2. Study Area

The study focuses on a mountainous watershed of Bindal river in the Western Himalayan state of Uttarakhand. The Bindal River (78°1'6.087"E, 30°16'17.699"N) in the Lesser Himalayas is a relatively small watershed covering 44.4 km². Originating from the base of the Mussoorie ridges, the Bindal River is sustained by numerous springs and headwater streams. Serving as a tributary to the Ganga River, it traverses through Dehradun, the capital of Uttarakhand. It is characterized by rugged terrain, with a substantial elevation ranging from 539m to 997m Figure 1a).

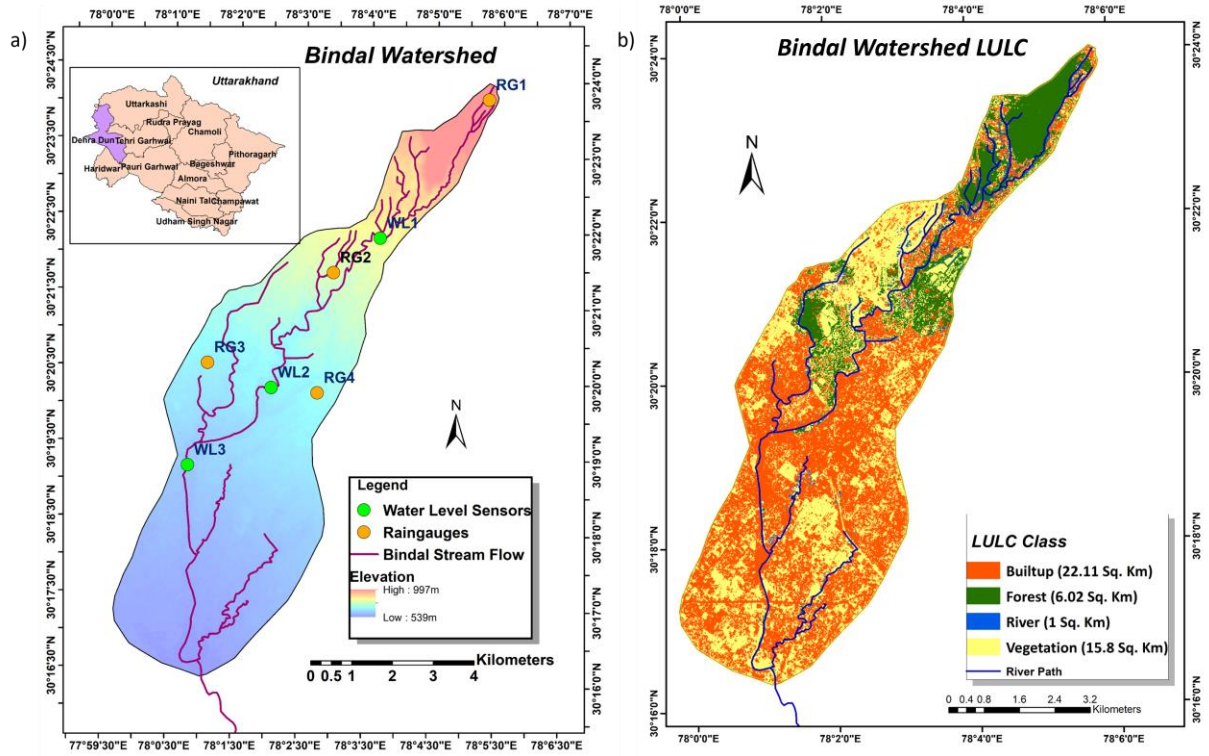

*Figure 1: Bindal Watershed. a) Map of Bindal watershed with sensor locations, i.e., rain gauges: RG1, RG2, RG3, RG4, and river water level recorders: WL1, WL2, and WL3; The **inset map** illustrates the location of the watershed within the broader Dehradun district boundary (shaded purple) in Uttarakhand state to provide regional geographical context. **b)** Land Use/Land Cover (LULC) classification of the Bindal watershed highlights the dominance of built-up areas (22.11 km²) and vegetation (15.8 km²) across the 44.4 km² Watershed.*

The Bindal River is ephemeral in nature, remaining dry or experiencing low flow throughout the year. However, the probability of FFs increases during the monsoon months or when sudden atmospheric depressions cause short bursts of heavy rainfall (Vanama et al., 2016). Riverside settlements are home to residents with limited incomes and restricted earning prospects. Due to the infrequent flow, riverine communities often perceive these rivers as less hazardous.

Consequently, over time, they encroach upon the riverbanks, gradually reducing the river's width and exposing human settlements to potential hazards (Bansal et al., 2015; Habeeb & Javaid, 2019).

3. Methodology

The methodology of the present work is divided into four key components, encompassing various stages that emphasize inclusiveness, a bottom-up approach, and accounting for hydrological dynamics. These stages range from initial engagement with stakeholders (local authorities and affected communities) to the analysis of collected hydrological data and the development of an efficient EWS (Figure 2). The first step involved interacting with local communities to understand their perception of flooding, identify flood-prone areas along rivers, and to foster trust in the EWS. In addition, the flood level thresholds were determined based on the observed impacts of water levels on the community. The second step involves real-time monitoring and data collection. Telemetry sensors are installed across the watershed to measure rainfall and river water levels, with their placement guided by community input and watershed topography. Further, satellite and reanalysis data are collected for comparative analysis. The third step focuses on watershed characterization throughland use and land cover analysis and assessment of rainfall variability. The observed data is compared with secondary sources to evaluate their reliability for integration into the EWS. The fourth step involves analyzing rainfall patterns and watershedresponse to characterize hydrological dynamics relevant to flood generation . These four key components are equally important and are operationally interlinked, forming a sequential and interdependent framework essential for the robustness and effectiveness of the EWS (Figure 2).

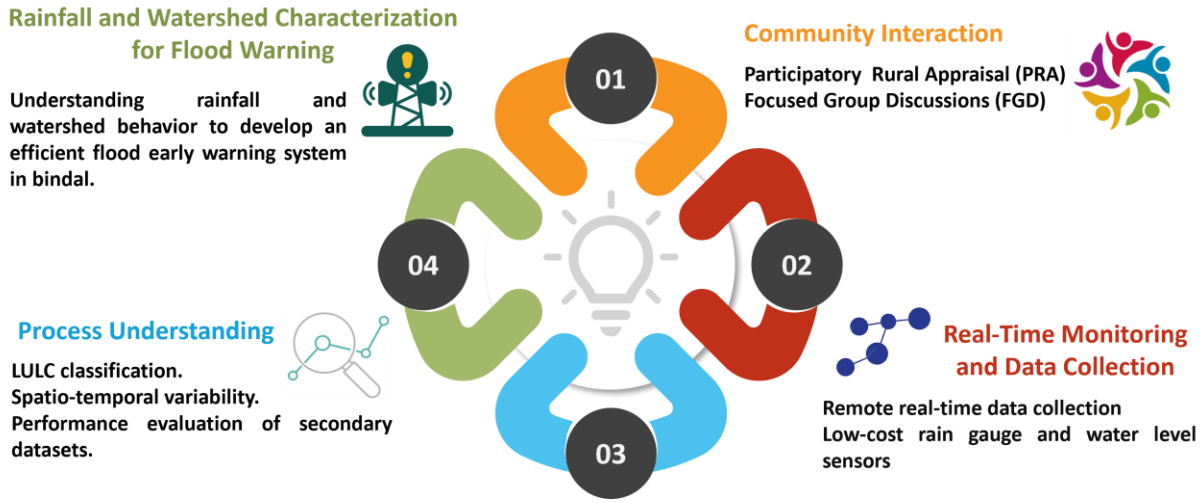

Figure 2 The key components of the methodology adopted in the present work.

3.1. Community Interaction

Effective communication with the community is essential for implementing an EWS. This involves understanding the community's perspective on flooding and its impacts. It helps enhance our understanding of context-specific risks, vulnerabilities, and exposure levels. Moreover, the community fosters a sense of ownership and builds trust in the EWS for floods. According to the transect survey conducted by the research team and discussions held with local stakeholders, the lower reach of the Bindal River is more severely affected by floods compared to its upper and middle reaches. Therefore, the lower reach of the Bindal river was further divided into three different stretches (as shown in Figure 3a) (i) from Kanwali Road Bridge to Laal Bridge – 1.82 km, (ii) from Laal Bridge to Bindal Bridge (located at Haridwar Bypass) - 2.11 km, and (iii) from Bindal Bridge (located at Haridwar Bypass) to Chandchak Bridge – 2.28 km. In addition to the above, another stretch covering a small tributary of Bindal i.e. from Kali Mandir (located at Kargi Patel Nagar Bypass Road) Bridge to Lohia Nagar –2.40 km, was also considered. For detailed community interactions, an area of 4.21 sq. km. was considered covering all the flood-prone areas of the neighborhood situated on both banks of the river, along the above stretches. These neighborhoods come under the 12 wards of Dehradun city.

Community consultations were also held with residents from different neighborhoods along both banks of the river, as per the above stretches. The communities in these neighborhoods primarily consist of households that have migrated and settled from Bihar, Uttar Pradesh, and other parts of Uttarakhand. .

Participatory Rural Appraisal (PRA) exercises (Reddy et al., 2016), along with Focus Group Discussions (FGDs) with concerned community and ward members from the concerned flood-affected colonies, including slums along the four mentioned stretches, were conducted to gather crucial information required to develop early warning systems for the Bindal watershed. The PRA exercises included temporal analysis (such as historical transects, trend diagramming, and seasonal diagramming), spatial analysis (including socio-resource mapping), and relationship analysis (Venn diagrams and Scoring and Ranking).). At each of the 4 locations between 20 and 30 households participated in these exercises.

Historical transects documented events related to development (such as the establishment of colonies, roads, public buildings, protection walls, bridges, and sewer lines) along the selected river stretches, tracing back to the last 60 years. Past floods, along with their severity, were also noted. The years 2006, 2013, and 2018 were recently reported as flood years, resulting in significant damage. FGDs around the historical transect further helped in understanding the impacts of the above developmental activities on the nature of floods and related losses (riverbank erosion, public and private property loss, and livelihood loss). Trend analysis recorded decadal changes over a 40-year period, which helped examine changes in encroachment, settlement density, rainfall behavior, river base flows, flood frequency, and flood severity, as well as their correlations. For seasonal diagramming, a month-wise matrix was developed with the help of residents to understand seasonal changes with respect to river flow and record peak flows. The peak flows were reported for the period July to September, depending upon rainfall in the upper reaches of the Bindal watershed. The base flow of the river was reported to have decreased in all the stretches over the last four decades. However, the frequency and intensity of floods were reported to have increased during the last two decades.

During FGDs, residents identified the more vulnerable sites within concerned colonies and most affected households and structures based on experiences of previous floods. Bank erosion during floods resulted in damage to public and private property. Lohiya Nagar and Mehboob Colony (located on the right bank) and Dehra Khas (located on the right bank), in the second stretch were identified as the worst affected colonies during floods. These colonies are situated just after the confluence of the tributary (passing through Patel Nagar) with the main Bindal river. The other flood prone localities identified were Sanjay Colony (on the left bank) in the first stretch and Chota Bharuwala (on the right bank) in the third stretch, both subjected to bank erosion.

FGDs were held to understand the role of different institutions and effectiveness of rendered services. Scoring and Ranking exercise was undertaken with the participants to understand the extent of flood damages (loss of home, livestock, other assets, and livelihoods) across different occupational categories, namely services, business, labour, and unemployed. Daily wage labor households residing in informal settlements with mud housing located near riverbanks experienced the most severe impacts across different river reaches. At the household level, the losses reported were in terms of damage to the houses, loss of livestock and even family members, and assets like utensils, bicycles, television, etc. The elderly people, those above 50 years, were more informative about the earlier status of the river, changes in rainfall behavior, encroachment along the river stretches, drainage and sewer systems, and occurrence of floods and related damages. The younger generation and middle-aged persons (20 –40 years old) provided information related to the role of different departments in river and flood management and were more interested in the flood EWS. Water inundation levels for past flood events were marked on the social-resource maps, which later helped in validating and determining the different levels of thresholds, warning, and actions required. The participants were also encouraged to identify sites where water level sensors and rain gauges need to be installed. .

According to the PRAs and FGDs conducted with the residents of neighborhoods located along the four selected stretches of the Bindal river, it was found that the severity of flood damages was much more in the second stretch (Laal Bridge to Bindal Bridge) as compared to third stretch (Bindal Bridge to Chandchak Bridge) and first stretch (Kanwali Road Bridge to Laal Bridge), in decreasing order. The neighborhoods along the fourth stretch were reportedly the least affected. A qualitative case-study research methodology was adopted, for which the five most vulnerable localities were further identified along the three stretches during the participatory resource mapping exercises. In each of these five localities, 20 households were selected in consultation with the ward members, considering differences in their sources of livelihoods (Services, Business, Labour, and Unemployed), to understand

the disparity of impacts during floods, if any. This resulted in a total sample size of 100 households for the case study of Bindal floods. These surveys helped identify the most affected households and understand the impact of flooding on them. It revealed that households with more unemployed members and income primarily from labour, living closer to the riverbanks, suffered the most through the loss of household assets and required more recovery time. .

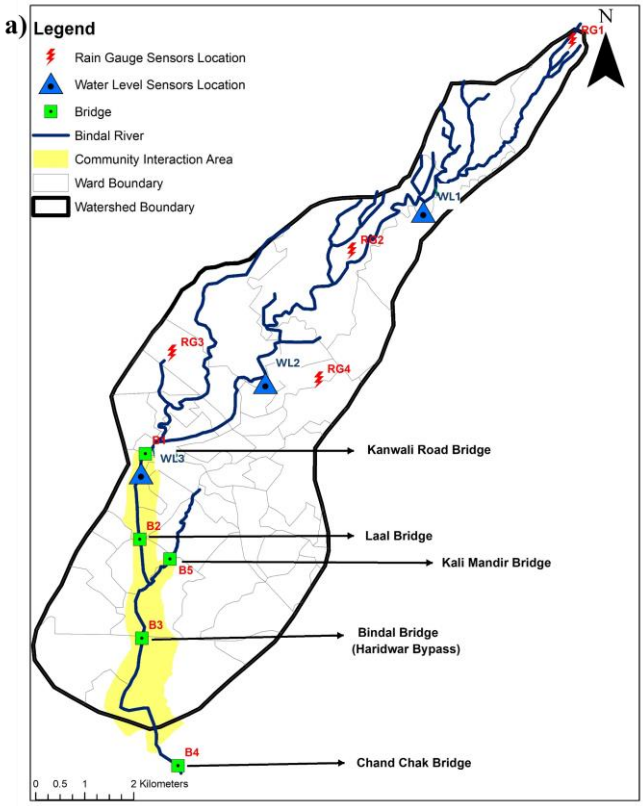

Figure 3a): Hydrological monitoring network of the Bindal River watershed. The map integrates ward boundaries with the locations of rain gauge (RG1–RG4) and water level (WL1–WL3) sensors, alongside key bridge infrastructure (B1–B5) and designated community interaction zones.

3.2. Real-Time Monitoring and Data Collection

In-Situ Sensor Data Collection

Real-time data collection used cost-effective telemetry rainfall and water level sensors strategically deployed to comprehensively understand rainfall dynamics and precisely capture variability within the Bindal River watershed. Lidar-based distance sensors were used for measuring water levels. Lidar ranging operates by utilizing the roughness of the reflective surface to produce nonspecular reflection, or scattering, of the laser beam. The application of Lidar for distance measurement is promising due to its cost-effectiveness, high energy efficiency, and minimal spatial footprint. The sensor can take measurements up to an incidence angle of approximately 40° with an accuracy of around 1 cm for distances less than 10 m. It also achieves a maximum detectable range of 30–35 m (Paul et al., 2020). The Davis tipping bucket rain gauge can measure rainfall levels ranging from 0 to 10.2 cm/hr, with a resolution of 0.2 mm and an opening diameter of 16.5 cm, covering a collection area of 214 cm^2 (Lanza et al., 2022).

Three Lidar-based water level sensors (WL1, WL2, WL3) were installed along the riverine length, and four tipping bucket rain gauges (RG1, RG2, RG3, RG4) were installed across the entire watershed at optimal locations (Figure 1a). Water level sensors WL1, WL2, and WL3 were located at the upper, middle, and lower sections of the watershed, respectively. Rain gauges are strategically positioned in the Bindal watershed to provide comprehensive coverage of rainfall variability across altitudinal zones. RG1, situated at the highest point, captures rainfall patterns in mountainous

terrain, while RG2, RG3, and RG4, positioned successively lower, provide data as rainfall moves between foothills and plains. This configuration provides a thorough explanation of the rainfall distribution and intensity gradients within the watershed. These telemetry water level sensors capture data every 5 minutes, while the telemetry rain gauges record rainfall at 15-minute intervals. Data collection commenced in September 2022. For seasonal analysis, rainfall data was divided into monsoon (JJAS) and non-monsoon periods (ONDJFMAM). Three distinct periods, late monsoon 2022, non-monsoon 2023, and monsoon 2023, were analyzed based on data availability.

Secondary Data Acquisition:

Sentinel-2 images of the study area from the European Space Agency Copernicus program were utilized for Level 1 Land Use/Land Cover (LULC) classification (Isbaex & Margarida Coelho, 2021). Optical data captured in September 2022 were obtained (Figure 1b), offering high spatial resolution (HR) imagery with a cloud cover of less than 0.08%. GPM (IMERG) Version 06- satellite data and ERA5 - the global atmospheric reanalysis data were utilized to evaluate the effectiveness of secondary rainfall data in capturing heterogeneity.(Hersbach et al., 2020; Skofronick-Jackson et al., 2017). In this study, we did not perform explicit bias correction or downscaling prior to comparison, as our objective was to assess the raw, inherent performance and biases of two readily available, high-temporal-resolution secondary rainfall products (GPM-IMERG and ERA5) relative to ground-observed rainfall. The rationale for this approach was to determine whether these global products, due to their accessibility and high temporal resolution, could adequately capture the variability and magnitude of precipitation within the smaller, topographically complex semi-urban Himalayan watershed.

3.3. Process Understanding

LULC Classification

Variations in land cover control the surface runoff mechanism and provide a better understanding of the study area. As the built-up area decreases, infiltration increases and surface runoff decreases, whereas an increase in forest area enhances infiltration and reduces surface runoff. Sentinel-2 images of 10 m spatial resolution were classified using ArcGIS 10.5's Maximum Likelihood (ML) supervised classification tool. Training data and spectral signature files were created to represent four uniform classes (Built-up, Forest, River, and Vegetation (including agriculture, scrubland, grassland)). All LULC maps produced using this technique have an accuracy of more than 80% (Ahmad & Quegan, 2013; Ali et al., 2019).

Spatio-temporal variability

Spatiotemporal variability analysis is crucial in hilly terrain due to the interplay of elevation, complex topography, and microclimate. Rapid elevation changes create localized weather patterns, while mountains can cause rain shadows and orographic effects. Therefore, rainfall and water level observations were analyzed to unveil spatial and temporal variability and characterize the watershed response. The observed rainfall as a function of distance, monthly cumulative rainfall observed at each rain gauge, and intraday variability during different periods capture spatial and temporal rainfall variability in the Bindal watershed. It is important to note that rain gauges with partial data availability are excluded from the comparison for that month.

Performance Evaluation of Secondary Datasets

In assessing the accuracy and capability of secondary datasets to capture rainfall dynamics, various descriptive indices (Table 1) were employed, including Percentage Bias (PBIAS), Root Mean Squared Error (RMSE), and cross-correlation. PBIAS gauges the average tendency of simulated datasets to overestimate or underestimate the reference dataset. By evaluating the dispersion of predicted values around observed data points, RMSE provides a concise measure of data performance. Cross-correlation between two timeseries measures the degree and nature of the relationship between them as they evolve. The value ranges between [-1,1]. By examining cross-correlation, potential dependencies and lead-lag relationships between variables can be identified, providing valuable insights into temporal associations and patterns. (Prakash, 2019; Prakash et al., 2012).

Table 1 Formulae used for various goodness of fit metrics.

Descriptive Indices	**Formulae**
Percent bias (PBIAS)	$\frac{\sum_{i=1}^{n}(Y_i^a - Y_i^b) \times 100}{\sum_{i=1}^{n}(Y_i^a)}$
Root mean square error(RMSE)	$\sqrt{\frac{1}{n}\sum_{i=1}^{n}(Y^a - Y^b)^2}$
Cross-Correlation (CC)	$\frac{\sum_{i=1}^{n}(Y_i^a - \overline{Y}^a)(Y_i^b - \overline{Y}^b)}{\sqrt{\sum_{i=1}^{n}(Y_i^a - \overline{Y}^a)^2} \times \sqrt{\sum_{i=1}^{n}(Y_i^b - \overline{Y}^b)^2}}$

Where Y_i, $\overline{Y}$, represents the rainfall, mean rainfall, and Y^a, Y^b, $\overline{Y}^a$, $\overline{Y}^b$ represent rainfall and mean rainfall of two different time series.

3.4. Rainfall and Watershed Characterization for Flood Warning

The watershed response to extreme rainfall patterns is a crucial factor to provide accurate and reliable flood warnings (Knighton & Walter, 2016). Therefore, the present section emphasizes understanding the association between extreme rainfall events and changes in the water level of the Bindal River. The observed water levels recorded within the watershed in response to different extreme rainfall events were classified into five types of alerts based on water level thresholds and corresponding actionable warning (Table2), using a threshold-based approach adapted from (Young et al., 2021). Water level thresholds are determined through a combination of statistical analysis and community involvement. Flood thresholds are determined by analyzing observed water level data to isolate extreme events, typically defined as values exceeding the 99th percentile. This percentile-based approach provides an objective criterion for identifying rare, high-impact flood occurrences. In addition to this, community engagement was undertaken to validate and refine the flood thresholds, integrating local knowledge and past experiences of flood events obtained through direct interaction with community members. Given the dynamic geomorphology of the narrow Bindal stream driven by anthropogenic factors such as waste material dumping, encroachment, and channel modification, a purely statistical approach to defining flood thresholds may be inadequate. These ongoing changes necessitate the integration of contextual and community-informed insights for more accurate flood characterization. The physical significance of these percentile-based thresholds is demonstrated by the varying hydrological responses captured across different river cross-sections and seasons. In this high-resolution dataset, comprising more than 200,000 water level timestamps, the numerical difference between the 99.9^{th} and 99.99^{th} percentiles represents significant hydrological variations despite the narrow range. For example, at monitoring site WL3 (width ~ 26 m), this 0.09% difference corresponds to a 0.27 m rise in water level, whereas at the narrower upstream site WL1 (width ~ 12 m), the difference increases to approximately 1.0 m. This ensures the system can distinguish between nuisance flooding and high-impact threats. Furthermore, the system manages 'out-of-scale' events by integrating community validation with statistical limits, ensuring the framework remains robust even during unprecedented flood events. And, as data collection continues, these observed datasets will grow, enabling the thresholds to become more robust over time.

Table 2 Five levels of flood alerts, their thresholds, and the action required.

Type of alert	Threshold	Action
Warning	99.99 percentile of Water level	Flood-like situation: Evacuate.
Advisory	99.9 percentile of Water level	Flood-like situation: Stay away from banks
Watch	99.5 percentile of Water level	Stay alert
Information statement	99 percentile of Water level	No action required
Cancellation	Below 99 percentile of Water level	Safety confirmed

A rainfall event is defined as a continuous period of rain lasting at least 30 minutes and any observations with minimum rainfall magnitude exceeding 2mm. By leveraging finer spatial and temporal resolutions, critical watershed dynamics, including rainfall storm movement direction, watershed response patterns, and rainfall trends, were studied. These insights are invaluable for developing an effective EWS.

To understand the severity of the rainfall, the daily rainfall has been classified into different categories based on its magnitude (Table 3). The India Meteorological Department (IMD) a national agency responsible for meteorological observations and weather forecasting, has established a classification system for rainfall severity based on its magnitude (Bhatla et al., 2019).

Table 3 Classification of daily rainfall based on IMD (India Meteorological Department) criteria. (source: (Bhatla et al., 2019))

Rainfall classification	Daily rainfall(mm)
No rainfall	0
Very light rainfall	0-2.4
Light rainfall	2.5-7.5
Moderate rainfall	7.6-35.5
Rather heavy rainfall	35.6-64.4
Heavy rainfall	64.5-124.5
Very heavy rainfall	124.6-244.4

4. Results and Discussion

4.1. Community involvement

Participatory Rural Appraisal (PRA) activities and Focus Group Discussions (FGDs) conducted with the local communities in the study area helped in gaining insights into the nature of floods. Below listed are the key findings from these exercises.

- The base flow of the river has decreased in the last 40 years. The water level in the river increases in the rainy season (July-Sept) up to 10-15 feet, but it remains as low as 0.5-1 feet throughout the year.

- The frequency and intensity of floods have been increasing over the last two decades, especially in the past 3-4 years attributed to intensified rainfall events. According to the locals, in the last 15 years there had been three major floods (2006, 2013 & 2018) with devastating impact.
- The human settlement along the banks of the Bindal River has increased since the 1970s. Encroachment on the riverbed was reported in all the stretches, reducing the width of the main course, which was identified as one of the major reasons for high flood intensity.
- In the stretch between Bindal Bridge and Chanchak Bridge (Figure 3), illegal riverbed mining activity is carried out throughout the year (except during the rainy season) on the left bank.
- Localities near the riverbanks remain at extreme risk during the monsoon. Damage caused by flooding was mostly in the form of bank erosion and breakdown of retaining walls, affecting public and private property.
- Retaining walls at numerous locations (Gandhi Gram, Sanjay Colony, Sangam Vihar, Sattowali Ghati, Dhera Khas, Kabadi Market, Muslim Colony and Chandchak) are damaged frequently following rainfall. One of the many high-tension wire towers constructed along the Bindal River from Kanwali Road Bridge to Laal Bridge stretch collapsed in the year 2018.

b)

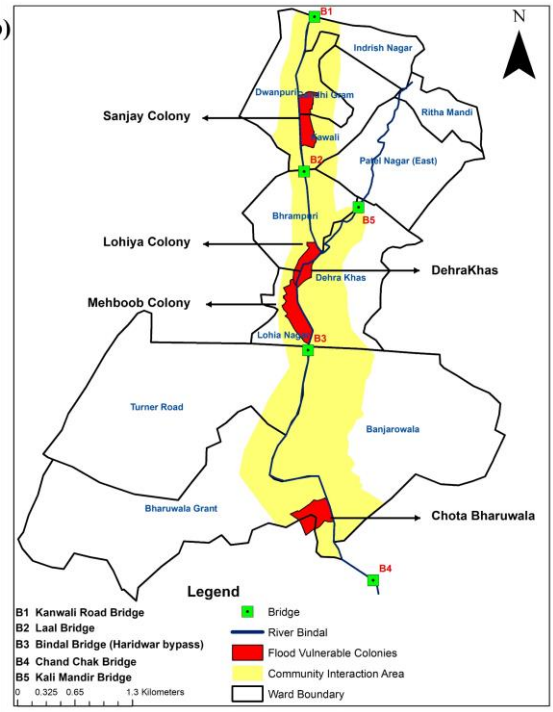

Figure 3b) *Detailed view of the Bindal River segment showing the proximity of flood-vulnerable colonies to the riverbed. The map illustrates the 100m community interaction buffer (yellow), key bridge infrastructure (B1–B5), and residential areas at high risk of seasonal flash flooding*

These findings highlight certain areas where the extent and impact of flooding are significantly greater than in other localities. Out of the 21 colonies surveyed (8 on the left bank and 13 on the right bank), five colonies—Sanjay Colony and Dhera Khas Basti on the left bank, and Lohia Nagar, Mehboob Colony (also known as Kabadi Basti), and Chota Bharuwala on the right bank were identified as the most vulnerable. These flood-prone areas, identified through PRA and FGDs, are useful for selecting appropriate locations for water level monitoring installations.

Another key observation is that the factors contributing to floods in the Bindal River area align with findings from previous studies. As noted by (Gaur et al., 2020), Bindal functions as a stormwater channel, but its condition is deteriorating primarily due to household waste (garbage) dumping, especially plastics, which significantly reduces the flow capacity of the drainage channels. Similarly, (Bansal et al., 2015) highlighted that river flooding is largely driven by garbage dumping and encroachments, while flooding in other parts of the city is due to inefficient stormwater drainage. These findings suggest that relying solely on conventional hydrological or hydraulic models with static thresholds for flood warning may not be effective. This is because such thresholds are highly sensitive to local conditions, such as the accumulation of debris in river channels. Therefore, thresholds should be determined at the local level and updated regularly in response to changes in channel morphology. Overall, these insights reinforce the importance of localized flood risk assessment and adaptive threshold-setting to improve the effectiveness of EWSs in the Bindal River context.

4.2. Spatio-temporal variability

The spatial variability of rainfall is illustrated through a cumulative monthly rainfall analysis, as depicted in Figure 4. Months with cumulative rainfall greater than 200 mm are shown. Plots for all the months can be found in the Supplementary Information (figure S1). Figure 4 shows significant variations in cumulative rainfall, showcasing distinct rainfall patterns observed within the watershed. During the late monsoon period in September 2022, there was

a significant 187 mm difference between RG1 (higher elevation) and RG4 (lower elevation). Additionally, during the non-monsoon period from January 2023 to May 2023, cumulative rainfall differences across the rain gauges exceeded 200 mm. Higher elevations witness substantial total rainfall, which gradually decreases towards lower elevations. This trend persists for 5 out of 10 months, from September 2022 to June 2023, with RG1 showing higher rainfall, as seen in the supplementary Figure S1. These findings are coherent with existing literature. (Henn et al., 2018; Nogueira, 2020; Shrestha et al., 2012) and can be attributed to orographic rainfall, where mountain barriers influence airflow and augment regional rainfall over lower hills (Kitchen & Blackall, 1992; Prat & Barros, 2010).

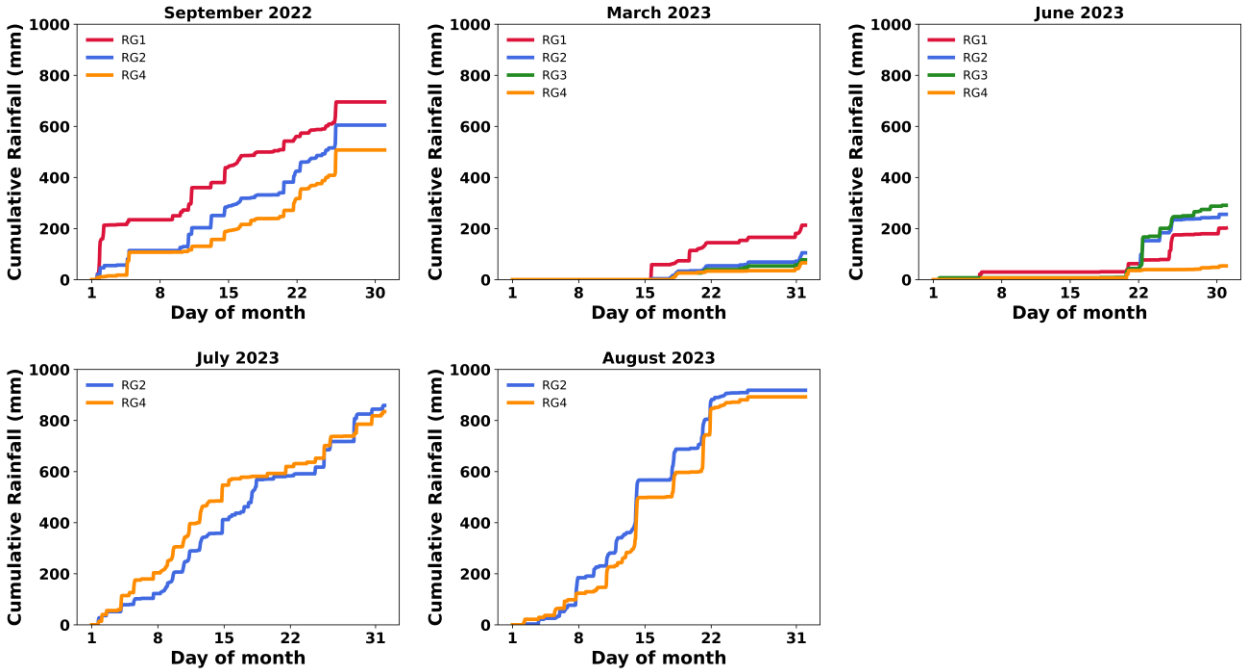

Figure 4: Cumulative plot of monthly observed rainfall across different rain gauges in the watershed (only months with more than 200 mm of cumulative rainfall are shown), illustrating spatial variability in rainfall. Higher elevations generally receive more rainfall than lower elevations. Additional plots for all months (September 2022–August 2023) are provided in the Supplementary Information (Figure S1).

The spatial variability of rainfall at the seasonal scale is illustrated in Figure 5, which presents a correlation analysis across different distances. The correlation coefficient was computed between pairs of rain gauges for each season and plotted against the distance (in kilometers) separating them. During the non-monsoon period, cross-correlation, representing the similarity between rain gauge time series, generally declined from 0.83 to 0.24 over distances ranging from 2.7 to 8.24 km. A similar trend was observed during the monsoon seasons of 2022 and 2023, where the correlation dropped from 0.55 (2022) and 0.70 (2023) to below 0.1 and 0.26, respectively, over the same distance. This indicates a sharper decrease in similarity during the monsoon season. The steeper slopes observed during the monsoon periods (0.086 and 0.081) suggest more rapid spatial rainfall variability than the non-monsoon period. Although it is well established consistent with Tobler's law that similarity in rainfall decreases with increasing distance (Pavlopoulos & Gupta, 2003), it is particularly noteworthy that significant variability is evident even across relatively short distances of up to 8 km within this small watershed.

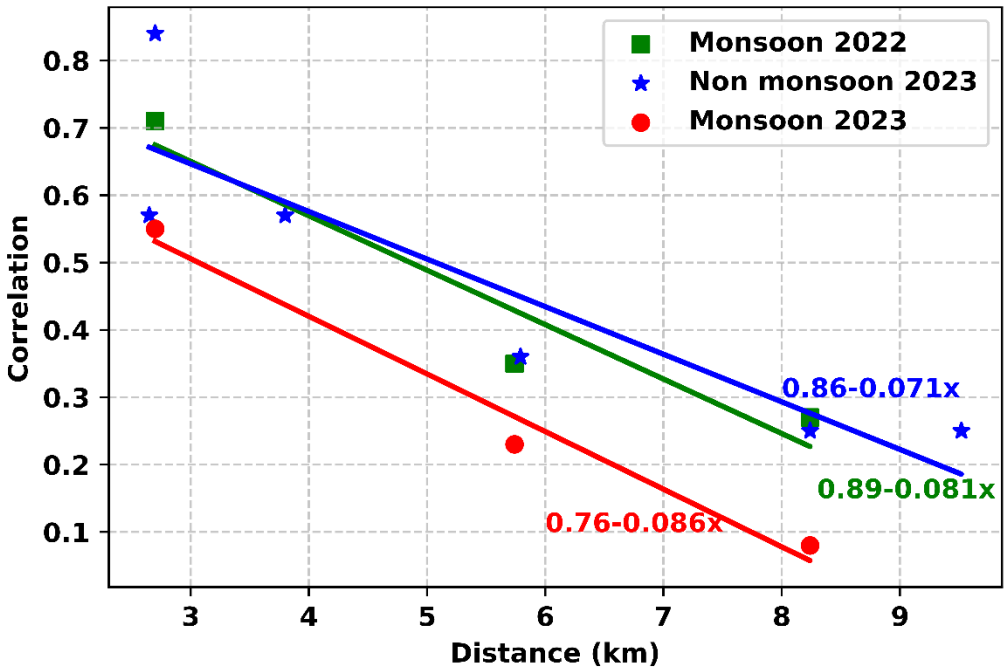

Figure 5: Correlation between rainfall observed at different rain gauges as a function of distance, analyzed at a seasonal scale. The plot highlights the rapid decline in similarity (high variability) over short distances within the watershed, particularly during the monsoon season.

The above analysis, shown in Figures 4 and 5, spotlights the pronounced spatial heterogeneity of rainfall within a relatively compact watershed, shaped by both topographic influences and seasonal dynamics. The cumulative rainfall differences, consistently observed across multiple months, and the sharp decline in inter-gauge correlation over short distances highlight the limitations of relying on sparse or single-point rainfall measurements in complex terrains. To robustly assess system variability, we analyze an extended dataset (August 2024–October 2025), which confirms the persistence of high-frequency spatial variability in rainfall across the four rain gauges (RG1–RG4), as shown in Supplementary Figure S3. Weekly rainfall differences between adjacent gauges frequently ranged from 50 mm to more than 200 mm, with RG1 consistently exhibiting the highest weekly rainfall peaks among all gauges. These results indicate that the localized rainfall dynamics observed during the primary study period represent persistent characteristics of the watershed, rather than isolated or anomalous events. These findings emphasize the importance of high-resolution spatial rainfall monitoring, particularly for hydrological modeling, flood forecasting, and water resource management in mountainous or orographically influenced regions (Buytaert et al., 2006; Z. Li et al., 2014; Panziera et al., 2015) Ultimately, traditional methods relying on sparse gauge networks or uniform rainfall assumptions may lead to underestimation of flood hazards in such terrains. Integrating spatially distributed hydrological models that account for elevation-driven rainfall variability, along with real-time radar data and probabilistic forecasting techniques, can significantly enhance the accuracy and reliability of EWS in mountainous watersheds (Rafieeinasab et al., 2015).

4.3. Secondary Data Comparison

The high spatiotemporal rainfall variability observed within a small watershed highlights the necessity of employing high-resolution data to effectively capture such variability for hydrological modeling and understanding watershed dynamics. When a high density of observed data points are unavailable, alternative options, such as secondary datasets, become necessary. Therefore, their performance evaluation becomes an important task in obtaining reliable results.

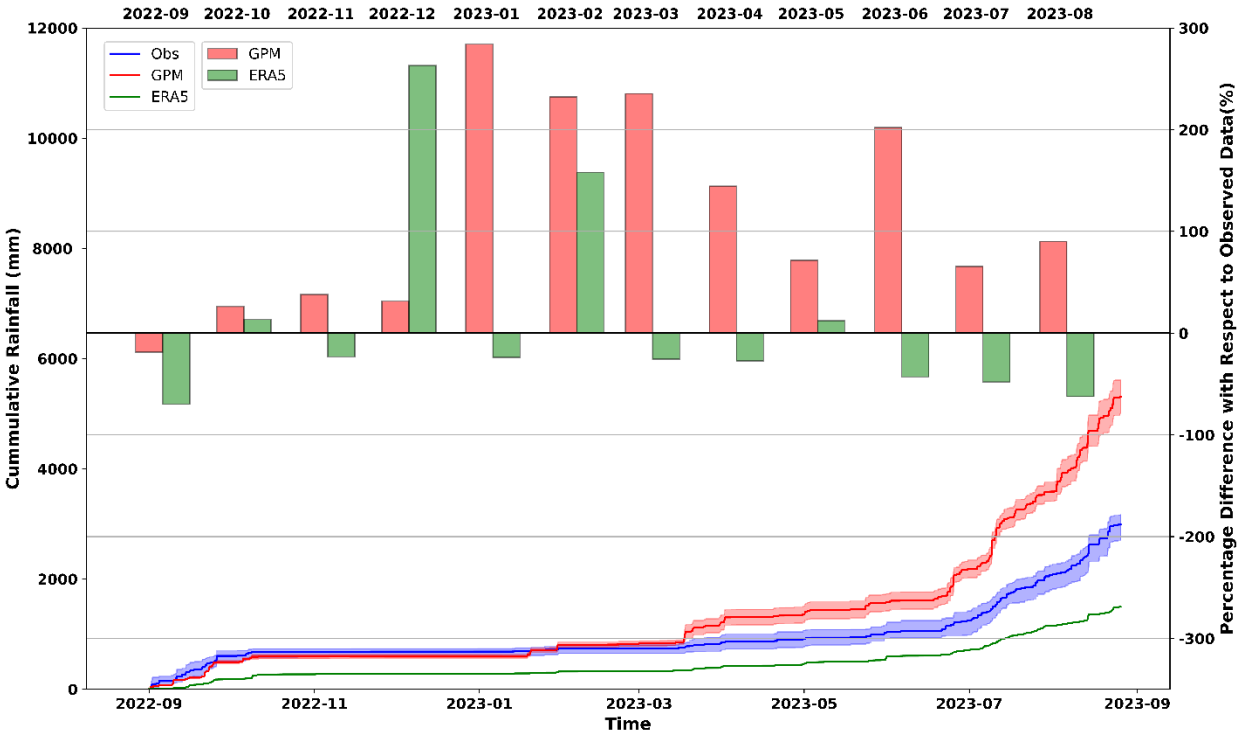

Figure 6 Comparison of cumulative rainfall and monthly percentage differences between observed gauge data (Obs), GPM, and ERA5 datasets from September 2022 to August 2023. The lower panel shows cumulative rainfall (mm), where the solid lines represent the spatial average and the shaded regions indicate the range between the minimum and maximum rainfall values across all pixels and gauges within the basin. The upper panel displays the monthly percentage difference of GPM (red bars) and ERA5 (green bars) relative to the observed data.

Figure 6 compares cumulative rainfall between observed and secondary datasets from late monsoon 2022 to monsoon 2023. Further, it illustrates the monthly percentage difference in cumulative rainfall between the observed data and the secondary data. The ERA5 dataset has a resolution of 0.25° × 0.25°, covering the watershed area within a single pixel. In contrast, the GPM data utilizes a higher resolution of 0.1° × 0.1°, resulting in two pixels covering the watershed. The observed data is derived from four rain gauges. The graph displays ERA5, GPM, and observed data, with spatial variability represented by shaded areas.

Upon comparing the secondary datasets, it becomes evident that neither the satellite nor the reanalysis adequately represents the rainfall of this watershed. However, during the monsoon period, ERA5 underestimates rainfall, with discrepancies exceeding 40% compared to observed monthly cumulative rainfall. Additionally, it demonstrates mixed behavior in the non-monsoon period, with significant percentage differences (>100%), particularly when cumulative monthly rainfall is low (<50 mm). These findings underscore ERA5's underestimation of rainfall throughout the year. Furthermore. For example, the percentage difference was around 200% in June, exceeding 70% on average.

Table 4 Statistical comparison of secondary rainfall (GPM-IMERG and ERA5) with observed rainfall

	GPM-IMERG	**ERA5**
PBIAS	-43.57	100.16
RMSE (Hourly rainfall)	3.65	2.24
CC (Hourly rainfall)	0.117	0.173
RMSE (Daily Rainfall)	32.95	18.36
CC (Daily rainfall)	0.488	0.456
Cumulative annual Rainfall (mm)	5306.53	1495.8

When compared to using descriptive indices in Table 4, ERA5 outperformed GPM in RMSE, with lower values of 2.24mm (hourly) and 18.36 mm (daily) compared to 3.65mm and 32.95mm, respectively. ERA5 also exhibited a higher correlation coefficient (0.173 for hourly rainfall) than GPM (0.117). However, GPM showed a higher correlation for daily rainfall. Despite these differences, both datasets displayed biases GPM overestimated rainfall while ERA5 underestimated it. The cumulative observed rainfall was 2994 mm. ERA5 shows less error and better captures the hourly pattern, while GPM effectively captures the daily rainfall pattern. Overall, ERA5 tends to overestimate light rainfall and underestimate moderate to heavy rainfall, while GPM exhibits the opposite behavior, tending to underestimate light rainfall and overestimate moderate to heavy rainfall (Chen et al., 2023; Xin et al., 2021).

Secondary rainfall data, while valuable, faces limitations in accurately capturing the heterogeneity of rainfall patterns, especially in regions with complex terrains and urban areas. It often fails to represent heterogeneity at higher temporal and spatial resolutions, as evidenced by correlation coefficients of 0.117 and 0.173 (Henn et al., 2018; Z. Zhou et al., 2019). Therefore, there is an urgent need for high-resolution, long-term rainfall datasets having spatial and temporal variability. This is critical to analyze the interplay between rainfall variability, watershed heterogeneity, and hydrological response in complex terrains and urban areas (Cristiano et al., 2017).

4.4. Watershed Dynamics and Warning

Rainfall and water level data were analyzed to understand watershed dynamics and their relationship with flood warnings. The peak rainfall intensity at 15-minute intervals was calculated for each rain gauge during three distinct periods: (a) Monsoon 2022, (b) Non monsoon 2023, and (c) Monsoon 2023. Figure 7 presents the probability density functions (PDFs) of the 15-minute maximum rainfall intensities recorded at each rain gauge for these different seasons. The Y-axis represents density, a smoothened estimate of the probability distribution of the data..

During the monsoon season, distinct patterns emerge in peak intensities across various rain gauges, while non-monsoon periods lack such clear trends. Within the monsoon season, there is a gradual increase in the magnitude of maximum intensity downstream, particularly when examining rare events such as the tail of the distribution or extreme values of density. In monsoon 2022, RG1 shows higher density at lower rainfall intensity (20-30 mm/hr), while RG2 and RG4 display more varied distributions with notable peaks around 30-50 mm/hr. The same trend of rising peak intensity magnitudes from RG1 to RG4 is observed in late monsoon 2023. For instance, RG1 shows a 15-minute maximum rainfall density tail in the range of 70-80 mm/hr, which increases downstream to a range of 120-140 mm/hr at RG3 and RG4. In contrast, during the non-monsoon period, mixed behavior is observed among RG2, RG3, and RG4, while RG1 shows the highest peak intensity, opposite to the behavior observed during the monsoon period. The observed rainfall patterns are in congruence with the existing literature, indicating less intense but more sustained rainfall in forest areas (Siyum, 2020), while in urban areas, more intense and shorter-duration rainfall events are observed (Yang et al., 2024). This observation suggests that urban areas located at lower elevations are more susceptible to experiencing higher-intensity events (Y. Li et al., 2020).

Figure 7: Density plots showing the distribution of maximum 15-minute rainfall intensities (mm/h) observed at various rain gauges across different seasons within the watershed. The plots highlight distinct seasonal patterns, with notable differences between monsoon and non-monsoon periods, and variations in intensity magnitudes across gauges and downstream locations.

In addition to peak rainfall intensities, understanding the rainfall storm's direction is crucial.to improve the lead time for early warning. Correlation between the rain gauges can be used to characterize the rainfall storm's movement within the watershed. Rainfall data from all four rain gauges, observed at 15-minute intervals, were correlated with each other at varying lags from 0 to 5, as tabulated in Table 5. The maximum correlation was found at lag 1, equivalent to a 15-minute delay. Notably, there was a significant increase in correlation between RG1 and RG3/RG4 at lag 1, indicating a stronger association between these rain gauges during rainfall events. Our observations showed a consistent southwest movement of rainfall storms originating from RG1 (point at the highest elevation) and progressing towards RG3, where urban settlements are predominant at lower elevations. This southwest movement is likely to be caused by the combined effects of orography, prevailing wind patterns, and the urban heat island. The orographic effect leads to increased rainfall at higher elevations, while prevailing winds may cause the downward movement of rainfall storms. Further, the urban heat island effect can alter local atmospheric conditions and airflow patterns, influencing the spatial distribution of rainfall within the watershed (Wu et al., 2021). These mechanisms contribute to the observed downward movement of rainfall storms within the watershed, impacting rainfall patterns and intensity in urban areas at the lower elevation. The interaction between storm motion and a basin drainage network directly affects flood peaks. For example, storms moving downstream (aligned with river flow) generate faster hydrological responses and higher peak discharges compared to upstream-moving storms (Amengual et al., 2021). This occurs because downstream-moving storms synchronize rainfall intensity with water accumulation in channels.

Table 5 Lagged correlation between observed rainfall of rainguages within the watershed. Rows in bold and italics highlight instances where the correlation coefficient initially increases with the time lag before subsequently decreasing.

Lag 0 (No Delay)	**Lag 1 (15-min Delay)**	**Lag 2 (30-min Delay)**	**Lag 3 (45-min Delay)**	**Lag 4 (60-min Delay)**	**Correlated Rainguage**	**Lagged Rainguage**
0.278	0.248	0.154	0.102	0.070	RG1-RG2	RG2
0.109	***0.129***	***0.120***	***0.088***	***0.063***	***RG1-RG3***	***RG3***
0.189	***0.190***	***0.094***	***0.055***	***0.044***	***RG1-RG4***	***RG4***
0.278	0.196	0.184	0.106	0.071	RG2-RG1	RG1
0.447	***0.495***	***0.401***	***0.350***	***0.273***	***RG2-RG3***	***RG3***
0.561	0.454	0.203	0.140	0.084	RG2-RG4	RG4
0.109	0.087	0.083	0.070	0.065	RG3-RG1	RG1
0.447	0.309	0.200	0.140	0.121	RG3-RG2	RG2
0.343	0.186	0.131	0.119	0.085	RG3-RG4	RG4
0.189	0.112	0.095	0.062	0.051	RG4-RG1	RG1
0.561	0.371	0.206	0.110	0.067	RG4-RG2	RG2
0.343	***0.360***	***0.258***	***0.152***	***0.132***	***RG4-RG3***	***RG3***

The observed rainfall at all the rain gauges has been categorized according to the IMD criteria (Table 3), and the frequency of each rainfall category is presented in Table 6 below. The missing data was assumed to have zero rainfall and hence categorized as 'No Rainfall.' There were 21 days with heavy rainfall and 5 days classified as very heavy rainfall, which are recognized as potential causes of FFs.

Table 6 Classification of rainfall based on IMD criteria. The table displays the number of days associated with different categories of rainfall.

	No rainfall	**Very light**	**Light**	**Moderate**	**Rather heavy**	**Heavy**	**Very heavy**
RG1	243	40	39	20	12	4	1
RG2	231	26	50	18	24	8	2
RG3	288	17	29	14	8	3	-
RG4	244	19	53	22	13	6	2

Understanding the response time of the watershed is crucial for the effective operation of flood warning systems. Utilizing a lagged correlation method and comparing the time difference between peak rainfall and peak water level, it was determined that the watershed exhibits a range of response times from 15 minutes to 2 hours and 30 minutes. Specifically, this response time varies from 15 to 45 minutes during heavy and very heavy rainfall events. Out of the 26 days with heavy/very heavy rainfall recorded at one or more rain gauges (Table ST1), four days were selected to represent the complex watershed dynamics in response to the rainfall, as illustrated in Figure 8. A high degree of

rainfall distribution was observed, with some rain gauges recording heavy/very heavy rainfall while others recorded very light, light, and moderate rainfall. Further, it was observed that even for heavy/very heavy rainfall, flood warnings ranged from watch and advisory to warning levels, highlighting the role of complex watershed dynamics in addition to rainfall variability in predicting the severity of the flood.

Although Figure 8(a-d) is plotted for heavy/very heavy rainfall categories, strikingly different responses from the watershed are observed. In Fig. 8a, three rainfall spells with different durations and magnitudes occur, yet they produce nearly identical water-level responses, indicating that rainfall magnitude alone does not control the hydrological response. When examining the rainfall of all the rain gauges for 25/09/2022 and 21/08/2023 (Figure 8b, and 8d), we observe similar rainfall categories at RG1, RG2, and RG4 in both events all are in heavy and very heavy categories. On 25/09/2022, 73, 89, and 92.4 mm of rainfall were recorded in RG1, RG2, and RG4, respectively, while on 21/08/2023, 106.8, 167.6, and 242.2 mm of rainfall were recorded in RG1, RG2, and RG4. Despite being in the heavy/very heavy category, the magnitude of rainfall on 21/08/2023 was more severe. However, in contrast, the water level at WL3 downstream increased more on 25/09/2022, crossing the warning threshold, which is greater than the water level of WL3 on 21/08/2023, which only crossed the advisory threshold.

Further, it is interesting to note that on July 17th, 2023, RG2 and RG3 recorded heavy rainfall with magnitudes of 76.8 mm and 124.2 mm, respectively, while RG1 and RG4 simultaneously reported very light and light rainfall with amounts of 0.4 mm and 3.2 mm, respectively. This variation in rainfall distribution across the watershed resulted in a different response compared to the other three cases, with only a watch alert being issued. This underscores the importance of considering localized rainfall patterns and their impact on watershed dynamics when issuing flood alerts.

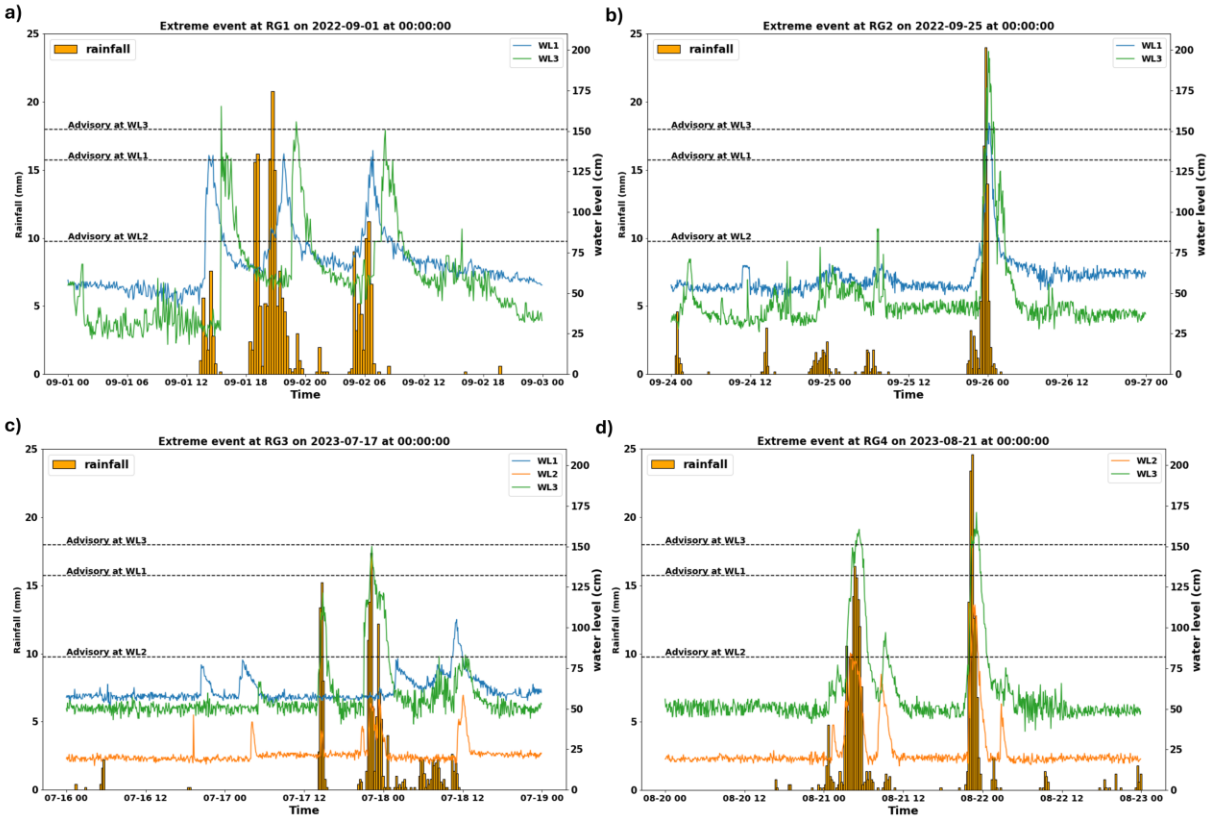

Figure 8 The response of water level sensors WL1, WL2, and WL3 to extreme rainfall events in the watershed, highlighting the variability in watershed dynamics. Advisory thresholds for water level alerts are indicated for each site (black dashed line). Panels a) to d) correspond to extreme rainfall events on different dates, showing the water level response and rainfall data from RG1 to RG4, respectively.

5. Conclusion

This study underscores the potential contribution of SMART approach of integrating low-cost, real-time watershed monitoring system with community-centric strategies to improve FEWS. Particularly in data-scarce, complex urban Himalayan settings of Bindal watershed, the inclusiveness and bottom-up approach of the SMART principle show the importance of community involvement in building an integrated approach to disaster risk reduction. Community participation helps gather on-ground information regarding the severity of floods, foster trust in the EWS, and identify vulnerable areas. This engagement also fostered a sense of responsibility and ownership, ensuring the optimal location and maintenance of sensor network. The community input was essential in defining flood-level thresholds as statistical methods alone may not suffice in dynamic watersheds like the Bindal, where human-induced changes alter the channel characteristics over time. Thus, integration of community-driven insights provide a responsive and context-specific approach to efficient FEWS. Rainfall and water level data from four rain gauges and three water level sensors were analyzed for characterizing the spatiotemporal variability of rainfall, storm movement, and watershed dynamics.

The detailed examination of extreme rainfall events sheds light on the watershed response to intense rainfall, revealing significant spatial and temporal variability in rainfall patterns within the 44.4 km^2 watershed. Higher elevations receive more rainfall, with a notable difference of 187mm observed in monthly rainfall between rain gauges situated 8.28 km apart, while lower elevations experience higher-intensity rainfall compared to higher elevations. Additionally, the work compares the performance of secondary data with observed rainfall using descriptive metrics such as PBIAS, RMSE, and correlation coefficient, revealing inadequacies in both satellite and reanalysis data representation of rainfall in this watershed. ERA5 underestimates, while GPM data overestimates rainfall, emphasizing the need for a high-resolution monitoring network for reliable FEWS in regions with complex terrains and urban areas. Our results also indicate that rainfall storms tend to move southwest downstream, with a lag of approximately 15 minutes observed between RG1 and RG3. The urban mountainous region exhibits complex hydrological behavior, where flood occurrences are influenced not only by meteorological factors, such as upstream rainfall patterns, but also by watershed-specific characteristics. Therefore, relying solely on heavy or very heavy rainfall at a single gauging point may be insufficient for accurate flood prediction and management in such terrains. These findings shows the critical importance of analyzing both rainfall patterns and watershed responses to extreme events for enhancing FEWS. Notably, the study demonstrates that small watersheds can exhibit rapid responses even to minor rainfall inputs. This highlights the need to consider watershed-scale variability and dynamics in hydrological assessments to support more effective flood management strategies.

Watersheds are inherently complex systems, where interactions among topography, land cover, and rainfall govern water flow and flood behavior. A comprehensive understanding of these dynamics, including rainfall patterns and runoff generation, enables better anticipation of and response to FF events. Such insights support the identification of vulnerable areas, the development of accurate flood models, and the timely issuance of warnings, ultimately strengthening community safety and resilience. Thus, integrating low-cost monitoring systems with hydrometeorological analysis and community engagement is essential for developing holistic EWS. These systems must not only be data-driven and responsive to watershed dynamics but also inclusive of community knowledge and participation.

6. Data availability

The rainfall and water level datasets collected through field instrumentation are not publicly available but can be obtained from the corresponding author upon request.

7. Author contributions

SD: Study conception and design, literature review, data collection, analysis and interpretation of results, and draft manuscript preparation. SS, KK, and DMH: Contributed to study conception and design, and provided feedback to refine the interpretation of results. All other authors: Reviewed the results, provided feedback to improve interpretation, and contributed to drafting the manuscript.

8. Competing interests

The authors declare that they have no conflict of interest.

9. Acknowledgements

The authors sincerely thank the Natural Environment Research Council (NERC) for financial support under grant no. NERC COP26 A&R, Project Scoping Call-2021COPA&R31Hannah. We are also grateful to the Centre of Excellence in Disaster Mitigation and Management (CoEDMM), IIT Roorkee, for providing essential resources, facilities, and support that were instrumental to this research. The first author gratefully acknowledges the support of the Prime Minister's Research Fellowship (PMRF), Grant No. 2802448. We also extend our special thanks to Prof. Srikrishnan from CoEDMM for his valuable discussions and insightful input on the manuscript.

10. Financial support

This research has been supported by the Natural Environment Research Council (grant no. NERC COP26 A&R, Project Scoping Call-2021COPA&R31Hannah).

11. References

Ahmad, A., & Quegan, S. (2013). Comparative analysis of supervised and unsupervised classification on multispectral data. *Applied Mathematical Sciences*, *7*, 3681–3694. https://doi.org/10.12988/ams.2013.34214

Ali, S., Biermanns, P., Haider, R., & Reicherter, K. (2019). Landslide susceptibility mapping by using a geographic information system (GIS) along the China–Pakistan Economic Corridor (Karakoram Highway), Pakistan. *Natural Hazards and Earth System Sciences*, *19*(5), 999–1022. https://doi.org/10.5194/nhess-19-999-2019

Amengual, A., Borga, M., Ravazzani, G., & Crema, S. (2021). The role of storm movement in controlling flash flood response: an analysis of the 28 September 2012 extreme event in Murcia, southeastern Spain. *Journal of Hydrometeorology*. https://doi.org/10.1175/JHM-D-21-0001.1

Arlikatti, S., Maghelal, P., Agnimitra, N., & Chatterjee, V. (2018). Should I stay or should I go? Mitigation strategies for flash flooding in India. *International Journal of Disaster Risk Reduction*, *27*, 48–56. https://doi.org/10.1016/j.ijdrr.2017.09.019

Bansal, N., Mukherjee, M., & Gairola, A. (2015). Cause and impact of urban flooding in Dehradun. *International Journal of Current Research*, *7*(02), 12615–12627.

Bhatla, R., Verma, S., Pandey, R., & Tripathi, A. (2019). Evolution of extreme rainfall events over Indo-Gangetic plain in changing climate during 1901–2010. *Journal of Earth System Science*, *128*(5), 120. https://doi.org/10.1007/s12040-019-1162-1

Bloschl, G., Reszler, C., & Komma, J. (2008). A spatially distributed flash flood forecasting model. *Environmental Modelling & Software*, *23*(4), 464–478. https://doi.org/10.1016/j.envsoft.2007.06.010

Buytaert, W., Celleri, R., Willems, P., Bièvre, B. De, & Wyseure, G. (2006). Spatial and temporal rainfall variability in mountainous areas: A case study from the south Ecuadorian Andes. *Journal of Hydrology*, *329*(3–4), 413–421. https://doi.org/10.1016/j.jhydrol.2006.02.031

Chawla, I., & Mujumdar, P. P. (2020). Evaluating rainfall datasets to reconstruct floods in data-sparse Himalayan region. *Journal of Hydrology*, *588*, 125090. https://doi.org/10.1016/j.jhydrol.2020.125090

Chen, Y., Ding, M., Zhang, G., Wang, Y., & Li, J. (2023). Evaluation of ERA5 Reanalysis Precipitation Data in the Yarlung Zangbo River Basin of the Tibetan Plateau. *Journal of Hydrometeorology*, *24*(9), 1491–1507. https://doi.org/10.1175/JHM-D-22-0229.1

Collier, C. G. (2007). Flash flood forecasting: What are the limits of predictability? *Quarterly Journal of the Royal Meteorological Society*, *133*(622), 3–23. https://doi.org/10.1002/qj.29

Cristiano, E., ten Veldhuis, M.-C., & van de Giesen, N. (2017). Spatial and temporal variability of rainfall and their effects on hydrological response in urban areas – a review. *Hydrology and Earth System Sciences*, *21*(7), 3859–3878. https://doi.org/10.5194/hess-21-3859-2017

Das, J., Manikanta, V., Nikhil Teja, K., & Umamahesh, N. V. (2022). Two decades of ensemble flood forecasting: a state-of-the-art on past developments, present applications and future opportunities. *Hydrological Sciences Journal*, *67*(3), 477–493. https://doi.org/10.1080/02626667.2021.2023157

Dimri, A. P., Thayyen, R. J., Kibler, K., Stanton, A., Jain, S. K., Tullos, D., & Singh, V. P. (2016). A review of atmospheric and land surface processes with emphasis on flood generation in the Southern Himalayan rivers. *Science of The Total Environment*, *556*, 98–115. https://doi.org/10.1016/j.scitotenv.2016.02.206

Dogra, A., Thakur, J., & Tandon, A. (2023). Do satellite-based products suffice for rainfall observations over data-sparse complex terrains? Evidence from the North-Western Himalayas. *Remote Sensing of Environment*, *299*, 113855. https://doi.org/10.1016/j.rse.2023.113855

Flash Flood Guidance System (FFGS) with Global Coverage | World Meteorological Organization. (n.d.). Retrieved March 29, 2024, from https://community.wmo.int/en/hydrology-and-water-resources/flash-flood-guidance-system-ffgs-global-coverage

Gaur, A., Prakash, O., & Joshi, H. C. (2020). Comparative index for water pollution by rural and urban means. *The Pharma Innovation*, *9*(5), 359–365. https://doi.org/10.22271/tpi.2020.v9.i5g.4718

Gebrechorkos, S. H., Leyland, J., Dadson, S. J., Cohen, S., Slater, L., Wortmann, M., Ashworth, P. J., Bennett, G. L., Boothroyd, R., Cloke, H., Delorme, P., Griffith, H., Hardy, R., Hawker, L., McLelland, S., Neal, J., Nicholas, A., Tatem, A. J., Vahidi, E., … Darby, S. E. (2024). Global-scale evaluation of precipitation datasets for hydrological modelling. *Hydrology and Earth System Sciences*, *28*(14), 3099–3118. https://doi.org/10.5194/hess-28-3099-2024

Gu, X., Zhang, Q., Li, J., Singh, V. P., & Sun, P. (2019). Impact of urbanization on nonstationarity of annual and seasonal precipitation extremes in China. *Journal of Hydrology*, *575*, 638–655. https://doi.org/10.1016/j.jhydrol.2019.05.070

Habeeb, R., & Javaid, S. (2019). Social Inclusion of Marginal in the Great Climate Change Debate: Case of Slums in Dehradun, India. *SAGE Open*, *9*(1). https://doi.org/10.1177/2158244019835924

Hapuarachchi, H. A. P., Wang, Q. J., & Pagano, T. C. (2011). A review of advances in flash flood forecasting. *Hydrological Processes*, *25*(18), 2771–2784. https://doi.org/10.1002/hyp.8040

Henao Salgado, M. J., & Zambrano Nájera, J. (2022). Assessing Flood Early Warning Systems for Flash Floods. *Frontiers in Climate*, *4*. https://doi.org/10.3389/fclim.2022.787042

Henn, B., Newman, A. J., Livneh, B., Daly, C., & Lundquist, J. D. (2018). An assessment of differences in gridded precipitation datasets in complex terrain. *Journal of Hydrology*, *556*, 1205–1219. https://doi.org/10.1016/j.jhydrol.2017.03.008

Hersbach, H., Bell, B., Berrisford, P., Hirahara, S., Horányi, A., Muñoz-Sabater, J., Nicolas, J., Peubey, C., Radu, R., Schepers, D., Simmons, A., Soci, C., Abdalla, S., Abellan, X., Balsamo, G., Bechtold, P., Biavati, G., Bidlot, J., Bonavita, M., … Thépaut, J. (2020). The ERA5 global reanalysis. *Quarterly Journal of the Royal Meteorological Society*, *146*(730), 1999–2049. https://doi.org/10.1002/qj.3803

Hoang, D.-V., & Liou, Y.-A. (2024). Assessing the influence of human activities on flash flood susceptibility in mountainous regions of Vietnam. *Ecological Indicators*, *158*, 111417. https://doi.org/10.1016/j.ecolind.2023.111417

Isbaex, C., & Margarida Coelho, A. (2021). The Potential of Sentinel-2 Satellite Images for Land-Cover/Land-Use and Forest Biomass Estimation: A Review. In *Forest Biomass - From Trees to Energy*. IntechOpen. https://doi.org/10.5772/intechopen.93363

Jodar-Abellan, A., Valdes-Abellan, J., Pla, C., & Gomariz-Castillo, F. (2019). Impact of land use changes on flash flood prediction using a sub-daily SWAT model in five Mediterranean ungauged watersheds (SE Spain). *Science of The Total Environment*, *657*, 1578–1591. https://doi.org/10.1016/j.scitotenv.2018.12.034

Kitchen, M., & Blackall, R. M. (1992). Orographic rainfall over low hills and associated corrections to radar measurements. *Journal of Hydrology*, *139*(1–4), 115–134. https://doi.org/10.1016/0022-1694(92)90198-5

Knighton, J. O., & Walter, M. T. (2016). Critical rainfall statistics for predicting watershed flood responses: rethinking the design storm concept. *Hydrological Processes*, *30*(21), 3788–3803. https://doi.org/10.1002/hyp.10888

Kulkarni, S., & Agarwal, A. (2024). Quantifying the association between Arctic Sea ice extent and Indian precipitation. *International Journal of Climatology*, *44*(2), 470–484. https://doi.org/10.1002/joc.8337

Lanza, L. G., Cauteruccio, A., & Stagnaro, M. (2022). Rain gauge measurements. In *Rainfall* (pp. 77–108). Elsevier. https://doi.org/10.1016/B978-0-12-822544-8.00002-0

Lei, N., Gao, L., Liu, S., & Zhou, Z. (2024). The Spatiotemporal Clustering of Short-Duration Rainstorms in Shanghai City Using a Sub-Hourly Gauge Network. *Earth and Space Science*, *11*(3). https://doi.org/10.1029/2023EA003442

Li, Y., Fowler, H. J., Argüeso, D., Blenkinsop, S., Evans, J. P., Lenderink, G., Yan, X., Guerreiro, S. B., Lewis, E., & Li, X. (2020). Strong Intensification of Hourly Rainfall Extremes by Urbanization. *Geophysical Research Letters*, *47*(14). https://doi.org/10.1029/2020GL088758

Li, Z., Yang, D., Hong, Y., Zhang, J., & Qi, Y. (2014). Characterizing Spatiotemporal Variations of Hourly Rainfall by Gauge and Radar in the Mountainous Three Gorges Region. *Journal of Applied Meteorology and Climatology*, *53*(4), 873–889. https://doi.org/10.1175/JAMC-D-13-0277.1

Liu, B., Tan, X., Gan, T. Y., Chen, X., Lin, K., Lu, M., & Liu, Z. (2020). Global atmospheric moisture transport associated with precipitation extremes: Mechanisms and climate change impacts. *WIREs Water*, *7*(2). https://doi.org/10.1002/wat2.1412

Nanda, A., Sen, S., Jirwan, V., Sharma, A., & Kumar, V. (2018). Understanding plot-scale hydrology of Lesser Himalayan watershed—A field study and HYDRUS-2D modelling approach. *Hydrological Processes*, *32*(9), 1254–1266. https://doi.org/10.1002/hyp.11499

Nations, U., of Economic, D., Affairs, S., & Division, P. (2018). *World Urbanization Prospects The 2018 Revision*.

Nepal, S., Flügel, W.-A., & Shrestha, A. B. (2014). Upstream-downstream linkages of hydrological processes in the Himalayan region. *Ecological Processes*, *3*(1), 19. https://doi.org/10.1186/s13717-014-0019-4

Nogueira, M. (2020). Inter-comparison of ERA-5, ERA-interim and GPCP rainfall over the last 40 years: Process-based analysis of systematic and random differences. *Journal of Hydrology*, *583*, 124632. https://doi.org/10.1016/j.jhydrol.2020.124632

Panziera, L., James, C. N., & Germann, U. (2015). Mesoscale organization and structure of orographic precipitation producing flash floods in the Lago Maggiore region. *Quarterly Journal of the Royal Meteorological Society*, *141*(686), 224–248. https://doi.org/10.1002/qj.2351

Papalexiou, S. M., & Montanari, A. (2019). Global and Regional Increase of Precipitation Extremes Under Global Warming. *Water Resources Research*, *55*(6), 4901–4914. https://doi.org/10.1029/2018WR024067

Paul, J. D., Buytaert, W., & Sah, N. (2020). A Technical Evaluation of Lidar-Based Measurement of River Water Levels. *Water Resources Research*, *56*(4). https://doi.org/10.1029/2019WR026810

Pavlopoulos, H., & Gupta, V. K. (2003). Scale invariance of regional wet and dry durations of rain fields: A diagnostic study. *Journal of Geophysical Research: Atmospheres*, *108*(D8). https://doi.org/10.1029/2002JD002763

Prakash, S. (2019). Performance assessment of CHIRPS, MSWEP, SM2RAIN-CCI, and TMPA precipitation products across India. *Journal of Hydrology*, *571*, 50–59. https://doi.org/10.1016/j.jhydrol.2019.01.036

Prakash, S., Mahesh, C., Gairola, R. M., & Pal, P. K. (2012). Comparison of high-resolution TRMM-based precipitation products during tropical cyclones in the North Indian Ocean. *Natural Hazards*, *61*(2), 689–701. https://doi.org/10.1007/s11069-011-0055-7

Prat, O. P., & Barros, A. P. (2010). Ground observations to characterize the spatial gradients and vertical structure of orographic precipitation – Experiments in the inner region of the Great Smoky Mountains. *Journal of Hydrology*, *391*(1–2), 141–156. https://doi.org/10.1016/j.jhydrol.2010.07.013

Qian, Y., Chakraborty, T. C., Li, J., Li, D., He, C., Sarangi, C., Chen, F., Yang, X., & Leung, L. R. (2022). Urbanization Impact on Regional Climate and Extreme Weather: Current Understanding, Uncertainties, and Future Research Directions. *Advances in Atmospheric Sciences*, *39*(6), 819–860. https://doi.org/10.1007/s00376-021-1371-9

Rafieeinasab, A., Norouzi, A., Kim, S., Habibi, H., Nazari, B., Seo, D.-J., Lee, H., Cosgrove, B., & Cui, Z. (2015). Toward high-resolution flash flood prediction in large urban areas – Analysis of sensitivity to spatiotemporal resolution of rainfall input and hydrologic modeling. *Journal of Hydrology*, *531*, 370–388. https://doi.org/10.1016/j.jhydrol.2015.08.045

Rasmussen, K. L., & Houze, R. A. (2012). A Flash-Flooding Storm at the Steep Edge of High Terrain: Disaster in the Himalayas. *Bulletin of the American Meteorological Society*, *93*(11), 1713–1724. https://doi.org/10.1175/BAMS-D-11-00236.1

Reddy, K. S., Pankaj, P. K., Reddy, N. N., & Raju, N. S. (2016). Participatory Rural Appraisal in Drylands:A Holistic Approach for Getting Insight into an Agro-Ecosystem Analysis. *Journal of Rural Development*, *35*(4), 1–26.

Rentschler, J., Salhab, M., & Jafino, B. A. (2022). Flood exposure and poverty in 188 countries. *Nature Communications*, *13*(1), 3527. https://doi.org/10.1038/s41467-022-30727-4

Satendra, Gupta A. K., Naik V. K., Saha Roy T. K., Sharma A. K., & Dwivedi M. (2015). *Uttarakhand Disaster 2013* (pp. 1–184). National Institute of Disaster Management, New Delhi.

Shepherd, J. M., Carter, M., Manyin, M., Messen, D., & Burian, S. (2010). The Impact of Urbanization on Current and Future Coastal Precipitation: A Case Study for Houston. *Environment and Planning B: Planning and Design*, *37*(2), 284–304. https://doi.org/10.1068/b34102t

Shi, X., Chen, J., Gu, L., Xu, C.-Y., Chen, H., & Zhang, L. (2021). Impacts and socioeconomic exposures of global extreme precipitation events in 1.5 and 2.0 °C warmer climates. *Science of The Total Environment*, *766*, 142665. https://doi.org/10.1016/j.scitotenv.2020.142665

Shrestha, D., Singh, P., & Nakamura, K. (2012). Spatiotemporal variation of rainfall over the central Himalayan region revealed by TRMM Precipitation Radar. *Journal of Geophysical Research: Atmospheres*, *117*(D22). https://doi.org/10.1029/2012JD018140

Singh, O., Arya, P., & Chaudhary, B. S. (2013). On rising temperature trends at Dehradun in Doon valley of Uttarakhand, India. *Journal of Earth System Science*, *122*(3), 613–622. https://doi.org/10.1007/s12040-013-0304-0

Siyum, Z. G. (2020). Tropical dry forest dynamics in the context of climate change: syntheses of drivers, gaps, and management perspectives. *Ecological Processes*, *9*(1), 25. https://doi.org/10.1186/s13717-020-00229-6

Skofronick-Jackson, G., Petersen, W. A., Berg, W., Kidd, C., Stocker, E. F., Kirschbaum, D. B., Kakar, R., Braun, S. A., Huffman, G. J., Iguchi, T., Kirstetter, P. E., Kummerow, C., Meneghini, R., Oki, R., Olson, W. S., Takayabu, Y. N., Furukawa, K., & Wilheit, T. (2017). The Global Precipitation Measurement (GPM) Mission for Science and Society. *Bulletin of the American Meteorological Society*, *98*(8), 1679–1695. https://doi.org/10.1175/BAMS-D-15-00306.1

Song, X., Qi, J., Zou, X., Zhang, J., & Liu, C. (2022). Potential Effects of Urbanization on Precipitation Extremes in the Pearl River Delta Region, China. *Water*, *14*(16), 2466. https://doi.org/10.3390/w14162466

Upadhyay, D., Dixit, S., & Bhatia, U. (2023). Quantifying the Role of Internal Climate Variability and Its Translation from Climate Variables to Hydropower Production at Basin Scale in India. *Journal of Hydrometeorology*, *24*(3), 407–423. https://doi.org/10.1175/JHM-D-22-0065.1

US Department of Commerce, N. N. W. S. (n.d.). *Floods*. NOAA's National Weather Service. Retrieved May 4, 2024, from https://www.weather.gov/pbz/floods

Vanama, V. S. K., Dikshit, A. K., & Pandey, K. (2016). *Flood modelling with global precipitation measurement (GPM) satellite rainfall data: a case study of Dehradun, Uttarakhand, India* (A. M. Larar, P. Chauhan, M. Suzuki, & J. Wang, Eds.; p. 98801A). https://doi.org/10.1117/12.2223928

Wang, Z., Chen, X., Qi, Z., & Cui, C. (2023). Flood sensitivity assessment of super cities. *Scientific Reports*, *13*(1), 5582. https://doi.org/10.1038/s41598-023-32149-8

Ward, E., Buytaert, W., Peaver, L., & Wheater, H. (2011). Evaluation of precipitation products over complex mountainous terrain: A water resources perspective. *Advances in Water Resources*, *34*(10), 1222–1231. https://doi.org/10.1016/j.advwatres.2011.05.007

Wu, Y., Sun, J., Ying, Z., Xue, L., Chen, D., & Lin, W. (2021). Effects of Local-Scale Orography and Urban Heat Island on the Initiation of a Record-Breaking Rainfall Event. *Journal of Geophysical Research: Atmospheres*, *126*(16). https://doi.org/10.1029/2021JD034839

Xin, Y., Lu, N., Jiang, H., Liu, Y., & Yao, L. (2021). Performance of ERA5 reanalysis precipitation products in the Guangdong-Hong Kong-Macao greater Bay Area, China. *Journal of Hydrology*, *602*, 126791. https://doi.org/10.1016/j.jhydrol.2021.126791

Yang, L., Yang, Y., Shen, Y., Yang, J., Zheng, G., Smith, J., & Niyogi, D. (2024). Urban development pattern's influence on extreme rainfall occurrences. *Nature Communications*, *15*(1), 3997. https://doi.org/10.1038/s41467-024-48533-5

Yasmin, T., Khamis, K., Ross, A., Sen, S., Sharma, A., Sen, D., Sen, S., Buytaert, W., & Hannah, D. M. (2023). Brief communication: Inclusiveness in designing an early warning system for flood resilience. *Natural Hazards and Earth System Sciences*, *23*(2), 667–674. https://doi.org/10.5194/nhess-23-667-2023

Young, A., Bhattacharya, B., & Zevenbergen, C. (2021). A rainfall threshold-based approach to early warnings in urban data-scarce regions: A case study of pluvial flooding in Alexandria, Egypt. *Journal of Flood Risk Management*, *14*(2). https://doi.org/10.1111/jfr3.12702

Zakaria, M. I., & Jabbar, W. A. (2021). Flood Monitoring and Warning Systems: A Brief Review. *Journal of Southwest Jiaotong University*, *56*(3), 140–156. https://doi.org/10.35741/issn.0258-2724.56.3.12

Zhou, N., Hou, J., Chen, H., Chen, G., & Liu, B. (2024). A Rapid Forecast Method for the Process of Flash Flood Based on Hydrodynamic Model and KNN Algorithm. *Water Resources Management*, *38*(6), 1903–1919. https://doi.org/10.1007/s11269-023-03664-0

Zhou, Z., Smith, J. A., Wright, D. B., Baeck, M. L., Yang, L., & Liu, S. (2019). Storm Catalog-Based Analysis of Rainfall Heterogeneity and Frequency in a Complex Terrain. *Water Resources Research*, *55*(3), 1871–1889. https://doi.org/10.1029/2018WR023567